Bioactive Materials 13 (2022) 249–259

Contents lists available at ScienceDirect

Bioactive Materials

journal homepage: www.keaipublishing.com/en/journals/bioactive-materials

The protein corona modulates the inflammation inhibition by cationic nanoparticles *via* cell-free DNA scavenging

Xingliang Liu [a], Huiyi Liang [a], Yanzi Yan [a], Jingjiao Wu [a], Massimo Bottini [b,**], Lixin Liu [a,***], Yongming Chen [a,*]

[a] School of Materials Science and Engineering, Key Laboratory for Polymeric Composite and Functional Materials of Ministry of Education, Sun Yat-sen University, Guangzhou, 510275, China

[b] Department of Experimental Medicine, University of Rome Tor Vergata, Rome, 00133, Italy

ARTICLE INFO

Keywords:
Cationic nanoparticles
Cell-free DNA
Inflammation inhibition
Protein corona
Rheumatoid arthritis

ABSTRACT

A central paradigm in nanomedicine is that when synthetic nanoparticles (NPs) enter the body, they are immediately cloaked by a corona of macromolecules (mostly proteins) that mediates the role of the physicochemical properties in the NP biological functions (the "coronation paradigm"). In this work, we focused on the assessment of the "coronation paradigm" for cationic NPs (cNPs) used as rheumatoid arthritis (RA) drugs due to their ability to scavenge cell-free DNA (cfDNA). We fabricated series of cNPs uniformly coated with single or di-hydroxyl groups and different types of amino groups and showed that hydroxylated nanoparticles displayed a prolonged retention in inflamed joints and greater anti-inflammatory effect in collagen-induced arthritis (CIA) rats than the non-hydroxylated analogues. Especially, the cNPs with secondary amines and a di-hydroxyl shell showed the best performance among the tested cNPs. Proteomic analysis showed that the cNPs with a di-hydroxyl shell adsorbed less opsonin proteins than the cNPs carrying mono hydroxyl groups and non-hydroxylated ones, which may provide a mechanistic explanation for the different biodistribution profiles of cNPs. Thus, this study suggests that the protein corona mediates the effects of the surface chemistry on the fate and functions of cNPs as anti-RA drugs.

1. Introduction

Rheumatoid arthritis (RA), an autoimmune and systemic inflammatory disease characterized by chronic synovitis and persistent infiltration of inflammatory cells, is a serious health problem that affects about 1% of the worldwide population [1,2]. The pathophysiology of RA is coupled to an imbalance of the immune system, for example, cytokines, including TNF-α, IL-6, and IL-1β, are recruited to inflamed joints, triggering a cascade of events that would lead to the erosion of the bones, joints, and cartilages [3,4]. Thus, RA patients experience joint swelling and articular cartilage/bone destruction [5]. Current anti-RA drugs are mainly divided into four categories: disease-modifying anti-rheumatic drugs (DMARDs), glucocorticoids (GCs), non-steroidal anti-inflammatory drugs (NSAIDs), and biological agents [6]. However, the therapeutic effect of these drugs is still unsatisfactory because of the severe side effects and risk of immune suppression-mediated infections [7].

Recent studies have shown that cell-free DNA (cfDNA) released by dying cells are causative agents of RA [8–11]. For instance, it has been observed that cfDNA levels in the plasma of RA patients were much higher than those of osteoarthritis (OA) patients [12]. Additionally, the cfDNA levels in the joint cavity of RA patients were nearly 100 times of those of OA patients [13]. Sequencing of the molecular patterns of cfDNA in the synovial fluid of RA patients revealed that the oligonucleotides with hypomethylated CpG-motif sequences can provoke autoimmune responses [13]. As one of the damage-associated molecular patterns (DAMPs), cfDNA can bind to Toll-like receptor 9 (TLR9), a pattern recognition receptor (PRR) located on the endosomal membrane of immune cells, and activate innate immunity [14]. In general, cfDNA does not elicit inflammation due to its rapid degradation as well as its

Peer review under responsibility of KeAi Communications Co., Ltd.

* Corresponding author.
** Corresponding author.
*** Corresponding author.
E-mail addresses: massimo.bottini@uniroma2.it (M. Bottini), liulixin@mail.sysu.edu.cn (L. Liu), chenym35@mail.sysu.edu.cn (Y. Chen).

https://doi.org/10.1016/j.bioactmat.2021.10.044
Received 15 August 2021; Received in revised form 6 October 2021; Accepted 28 October 2021
Available online 3 November 2021

inability to access intracellular DNA sensors. However, the immune complexes (ICs) formed by the combination of cfDNA and self-nucleic acid antibodies/proteins (HMGB1, TFAM, LL37, and IL-26) can greatly avoid cfDNA degradation by nucleases [15–18]. After endocytosis by cells, cfDNA, or ICs, could interact with TLR9, or other nucleic acid receptors in the cells such as DNA-dependent activator of IFN-regulatory factor 1 (DAI) or retinoic acid-inducible gene (RIG) family members, and elicit the secretion of pro-inflammatory factors and induce immune cascades [19–21]. Thus, inhibiting the abnormal activation of nucleic acid receptors by eliminating cfDNA is an artful and feasible method for the treatment of inflammatory diseases.

Cationic materials that interact with negatively charged nucleic acids through electrostatic interactions may inhibit abnormal immune activation by cfDNA or their ICs. This assumption has been proven in some investigations, including acute liver failure, systemic lupus erythematosus, bacterial sepsis, psoriasis and RA [14,22–26]. Recently, we have illustrated that cationic nanoparticles (cNPs) formed by the self-assembly of poly(lactic-*co*-glycolic acid)-*b*-poly(2-(diethylamino) ethyl methacrylate) (PLGA-*b*-PDMA) had superior DNA binding affinity, co-localization with endosomes and *in vitro* blockade of inflammation than the soluble poly(2-(diethylamino) ethyl methacrylate) (PDMA) [25]. Additionally, we showed that cNPs could accumulate in the inflamed joints and paws and lead to a greater inhibition of joint swelling and restoration of destructed bone and cartilage in collagen-induced arthritis (CIA) rats than their soluble analogue [25]. In a follow-up study, we fabricated a library of cNPs with different charge densities by incorporating PEG segments into PLGA-*b*-PDMA with different block ratios. The introduction of PEG chains efficiently reduced the toxicity of cationic materials and prolonged the retention of cNPs in the joints, while preserving the ability to inhibit inflammation [27]. In this study we further explore cNPs by taking in consideration a crucial aspect of the behavior of NPs in the biologic milieu.

When NPs enter the biologic milieu, their surface is immediately cloaked by a corona of macromolecules (mostly proteins, but also lipids and carbohydrates), commonly referred to as "protein corona", which imparts a new "biologic identity" to the NPs. A central paradigm in nanomedicine is that the biologic identity mediates the effects of the physico-chemical properties (the "synthetic identity") on the biologic functions of the NPs (the "coronation paradigm"). Although this paradigm has been validated for several types of NPs used in the development of anti-cancer approaches [28], it has not been addressed for any type of NPs developed for the treatment of rheumatoid arthritis (RA). The application of the "coronation paradigm" to cNPs would suggest that, as soon as the nanoparticles are intravenously introduced in the body, plasma proteins adsorb onto their surface and impart a new biologic identity that affects their biologic functions, for instance, by hampering their ability to bind cfDNA and tagging them for removal [29]. Thus, it would be crucial to investigate the role of the protein corona in the inflammation inhibition by cNPs *in vivo*.

To the best of our knowledge, there has been no study to elucidate the influence of the protein corona on the biologic functions (*i.e.*, cfDNA scavenging capability) and biocompatibility of cNPs. It has been known that a hydroxyl-enriched shell can help to improve the biocompatibility and serum-tolerance of polycations *in vivo* [30,31]. To take advantage of

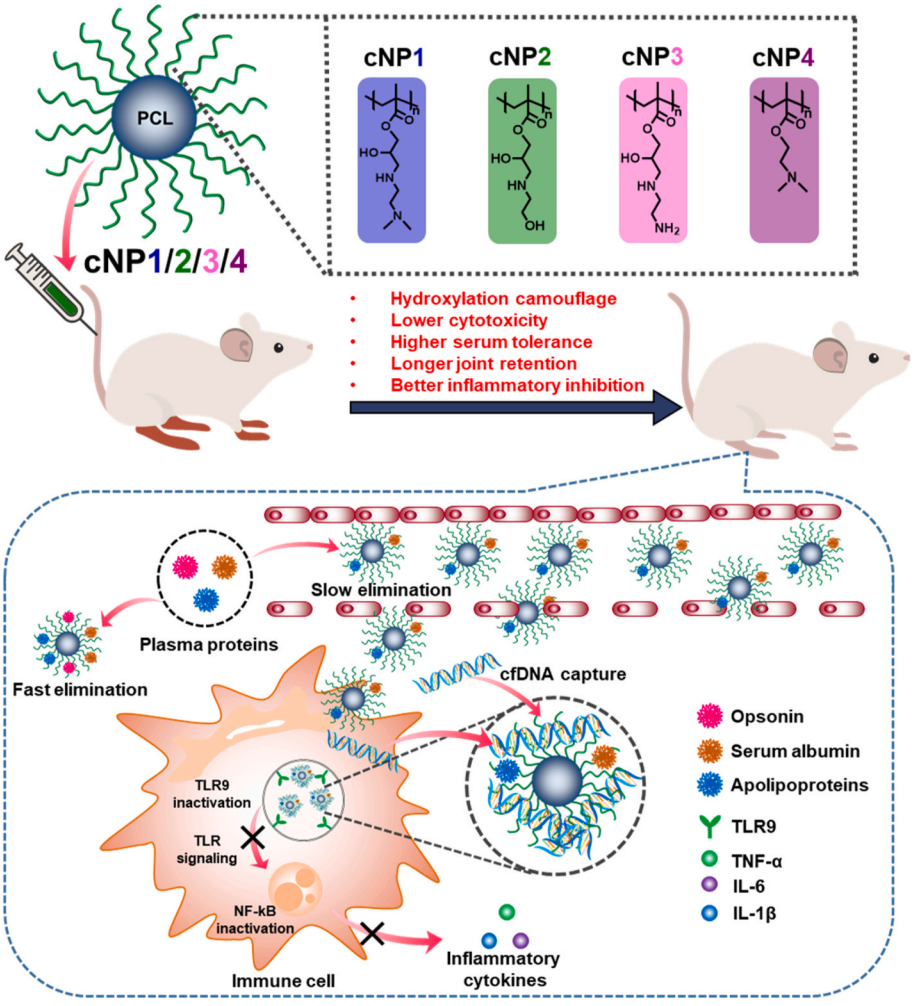

Scheme 1. Use of cNPs to inhibit immune cell activation and joint inflammation *via* cfDNA scavenging. cNP1-cNP3 had flanking hydroxyl groups, whereas cNP4, without flanking hydroxyl groups, was used as control. The cfDNA released from dying cells induced immune cell activation and joint inflammation. After intravenous injection into the CIA rats, cNP2 showed longer retention in the blood and inflamed paw joints and greater cfDNA scavenging than the other particles, which could be correlated to the lower adsorption of plasma proteins and different composition of the protein corona of cNP2. The improved biodistribution profile of cNP2 translated into a better anti-inflammatory effect.

this finding, we synthesized a series of poly(ε-caprolactone) (PCL) based di-block polymers carrying hydroxyl groups and different types of amino groups, including primary, secondary and tertiary (termed as cNP1, cNP2, and cNP3, respectively), by O-heterocyclic ring-opening reaction (Scheme 1). We showed that the presence of di-hydroxyl groups in PCL_{60}-*b*-$PGEA_{150}$ polymers improved the pharmacokinetic profile and cfDNA scavenging efficacy in joints of CIA rats of cNPs by decreasing plasma protein adsorption. Proteomic analysis of the cNPs' protein corona showed that a lower amount of fibrinogen, immunoglobulins, complement proteins and apolipoproteins adsorbed onto cNP2, suggesting a possible biologic mechanism mediating how the synthetic identity affects the fate of cNPs *in vivo* (Scheme 1).

2. Results

2.1. Fabrication and characterization of cNPs

Polycationic polymers with flanking hydroxyl groups exhibited lower cytotoxicity and superior gene transfection performances [32,33]. Thus, we fabricated and characterized cNPs carrying hydroxyl groups and different amine species. The di-block copolymers of poly(glycidyl methacrylate) (PGMA) with post-modifiable epoxy groups were applied to prepare hydroxylated cNPs. PCL_{60}-*b*-$PGMA_{150}$ was prepared *via* atom transfer radical polymerization of glycidyl methacrylate (GMA), and then modified with three types of amines (DMEN: N, N-dimethyl-1, 2-ethanediamine, EA: 2-aminoethanol and EDA: ethylenediamine) to achieve three different polymers (termed as PCL_{60}-*b*-$PGDMEN_{150}$, PCL_{60}-*b*-$PGEA_{150}$, and PCL_{60}-*b*-$PGEDA_{150}$) *via* epoxy ring-opening of GMA as described in Fig. S1. These polymers were characterized by hydrogen nuclear magnetic resonance (^{1}H NMR), Fourier transform infrared (FT-IR), and size exclusion chromatography (SEC) (Fig. S2 and Fig. S3). According to the integration ratio of the peaks at 4.04 ppm and 3.22 ppm (Fig. S3C), the ratio of polymerization degrees of PCL and PGMA was calculated to be 2:5. After post-modification, the disappearance of proton resonances at 3.22 ppm, 2.82 ppm, and 2.62 ppm (Fig. S4 and Fig. S5C) indicated that the epoxy groups were completely converted. The appearance of the stretching absorption peak of the hydroxyl group at 3400 cm^{-1} and the disappearance of the peaks of epoxy groups at 900 cm^{-1} and 845 cm^{-1} (Fig. S6) in the FT-IR spectra further validated the complete transformation of the epoxy groups by the nucleophilic reagents.

Three types of cNPs (cNP1, cNP2 and cNP3) with a hydroxyl shell were fabricated by the self-assembly of the corresponding block copolymers in an aqueous solution. Di-block copolymer PCL_{60}-*b*-$PDMA_{150}$ was also synthesized to prepare cNP4 devoid of surface hydroxyl groups (control). Transmission electron microscopy (TEM) showed that cNP1-cNP4 were spherical with a size of approximately 40 ± 5 nm (Fig. 1A). Dynamic light scattering (DLS) analysis showed that cNP1-cNP4 were well dispersed in phosphate-buffered saline (PBS) (1 ×, pH 7.4) as suggested by the monomodal distribution of hydrodynamic diameters. Interestingly, the introduction of the hydroxyl shell led to a slight decrease in the nanoparticles' hydrodynamic diameter as suggested by the different DLS traces of cNP4 *vs* those of cNP1-cNP3 (Fig. 1B). Conversely, the zeta potential of cNP1-cNP3 were comparable to that of cNP4, varying from 15 to 18 mV (Fig. 1C), indicating that the introduction of the hydroxyl shell did not lead to a significant reduction of the cNPs' surface charge (Table S2). Thus, three types of cNPs with shell containing different repeating units, cNP1 with one –OH group, one tertiary amine and one secondary amine, cNP2 with two –OH groups and one secondary amine, and cNP3 with one –OH group, one primary amine and one secondary amine, were obtained.

To evaluate whether the hydroxyl shell can improve the biocompatibility of cNPs, the cytotoxicity of cNPs to RAW 264.7 cells was evaluated by MTT assay (Fig. 1D). The IC75 of cNP1-cNP3 were 240 μg/mL, 209 μg/mL, and 230 μg/mL, respectively, whereas that of cNP4 was 62 μg/mL, which was significantly smaller than that of cNP1-cNP3. The low cytotoxicity of cNP1-cNP3 was attributed to the shielding effect of the hydroxyl shell, which reduced the exposure of cationic moieties to the cell membrane.

2.2. cfDNA scavenging efficacy of cNPs

Next, we investigated whether the addition of hydroxyl groups and different amine species affected the affinity of cNPs to cfDNA by evaluating the binding efficiency (BE) of cNP1-cNP4 to calf thymus DNA (ctDNA) by ethidium bromide (EtBr) competition assay. The amount of cNPs mixed with ctDNA was normalized based on the N/P ratio, *i.e.*, nitrogen atoms of cNPs to phosphorus of DNAs. The N/P ratio resulting in 50% of cNPs-DNA binding by EtBr competition assay was defined as BE50. Lower values of BE50 corresponded to a higher binding ability.

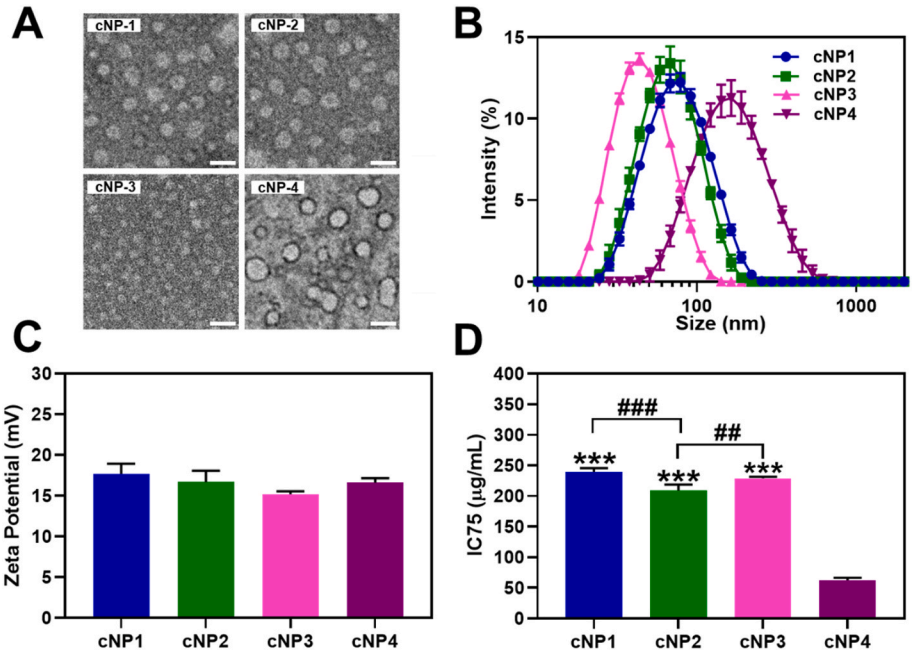

Fig. 1. Characterization of cNP1-cNP4. (A) Transmission electronic microscopy (TEM) images of cNP1-cNP4 (scale bar: 100 nm). Phosphotungstic acid was used as the negative-stain reagent. (B) Dynamic light scattering (DLS) traces of cNP1-cNP4 in PBS, (n = 3; means ± SD). (C) Zeta-potential of cNP1-cNP4 in PBS, (n = 3; means ± SD). (D) Cell viability (IC75) of RAW 264.7 cells treated with cNP1-cNP4 for 24 h (n = 3; means ± SD). Statistical significance was calculated by one-way ANOVA with the LSD post-test, ***$P <$ 0.001 versus cNP4. ##0.001 $< P <$ 0.01, ###$P <$ 0.001 between two groups.

The BE50 of cNP1 and cNP3 in PBS were 0.56 and 0.54, respectively (Fig. 2A). These two cNPs differ in the terminal amines and showed a slight difference in the efficiency of ctDNA binding. Conversely, the BE50 of cNP2 and cNP4 were 0.17 and 0.28, respectively. cNP2 and cNP4 contained a secondary and tertiary amine group, respectively, but cNP2 had also two hydroxyl groups. These results suggest that the secondary amine group had the highest efficiency of ctDNA binding under the same N/P ratio: despite the introduction of the two hydroxyl groups, the efficiency of ctDNA binding of cNP2 and cNP4 was not significantly different. Consistent results could be also seen by means of gel electrophoresis (Fig. S7). cNP1 and cNP3 efficiently bound CpG oligodeoxynucleotides at a N/P ratio of 8, showing a similar binding capability, whereas cNP2 and cNP4 bound CpG at a N/P ratio of 4 and 6, respectively. Thus, cNP2 with a secondary amine and two hydroxyl groups exhibited the best CpG binding affinity.

To mimic the *in vivo* scenario, 10% FBS was added to evaluate the BE50 between the cNPs and ctDNA in presence of serum proteins (Fig. 2B). The results showed that the BE50 of the cNPs increased due to the formation of a protein corona in serum, which weakened the electrostatic interactions between cNPs and ctDNA. It was noteworthy that the BE50 of cNP4 increased from 0.28 in PBS to 1.8 in presence of FBS (~6.5 fold increase), whereas, the BE50 of cNP1-cNP3 in 10% FBS were ~3, ~3.8 and ~3.7 times higher than those in PBS, suggesting that the affinity to ctDNA was more greatly influenced by the protein corona of cNP4 than that of cNP1-cNP3. Thus, the introduction of flanking hydroxyl groups may have tailored the adsorption of serum proteins onto the cNPs' surface in a way that did not significantly affect the nanoparticles' affinity to ctDNA. Significantly, cNP2 also showed the strongest ctDNA binding efficiency among the four cNPs in 10%FBS.

cfDNA generally combines with antibodies/proteins, including HMGB1, TFAM, LL37, and IL-26, in the tissue fluids to form immune complexes (ICs), which induce inflammation *via* the activation of TLR9 in immune cells [15]. To investigate whether the scavenging ability of cNPs is strong enough to extract cfDNA from ICs, we conducted competitive binding assay according to a procedure described previously [24]. First, FAM-labeled CpG was incubated with LL37 to form CpG-LL37 ICs. Then, cNPs with the same nitrogen content were added to the system and incubated for 30 min. The unbound LL37 and CpG-LL37 ICs could be separated through ultrafiltration. The cNP-CpG binary complex and cNP-CpG-LL37 ternary complex, if formed, were retained in the upper layer of the partition and quantitated by measuring FAM fluorescence intensity. As shown in Fig. 2C (solid line), the presence of cNP-CpG complexes increased with the nitrogen content, indicating a stronger interaction between cNPs and CpG. Among the four cNPs we tested, cNP2 showed the best binding ability to CpG. To confirm the presence of cNP-CpG-LL37 ternary complexes, the partition of LL37 was also evaluated by using FITC-labeled LL37. We found that the LL37 in the upper layer was less than 7% at low nitrogen contents (Fig. 2C dotted line), indicating that the cNP-CpG-LL37 complexes found in the upper layer were in a much less amount than the cNP-CpG complexes. These results implied that the interaction between cNPs and CpG outperformed that between LL37 and CpG, namely, the cNPs can extract CpG from the ICs with LL37 and could inhibit the activation of the TLR pathway. As shown in Fig. 2C, the LL37 binding efficiency of cNP4 was higher than that of cNP2 at all nitrogen contents, while cNP2 performed the best in extracting CpG from the ICs. These results agreed with the ethidium bromide (EtBr) competition assay between cNPs and ctDNA, indicating that, in the presence of proteins or ICs, cNP2 performed the best among the tested cNPs.

Then, we assessed the inhibition of CpG-induced TLR9 activation by cNPs with the same nitrogen content was assessed in Ramos Blue™ reporter cells (Fig. 2D). The results showed that all cNPs inhibited the activation of TLR9 by CpG in a dose dependent manner, demonstrating that cNPs could block the activation of TLR9 by CpG. Notably, cNP2 and cNP4 inhibited the activation of TLR9 to ~30% at a nitrogen content of 1.25 μg/mL, whereas cNP1 and cNP3 only to ~65%. These results agreed with the ethidium bromide (EtBr) competition assay between cNPs and ctDNA in PBS. Therefore, the cNP2 exhibited the most efficient inhibition of inflammatory among the cNPs we tested.

2.3. Therapeutic efficacy of cNPs in CIA rats

The above results showed that cNP2 exhibited a remarkable affinity with cfDNA and ability in extracting cfDNA from ICs, and a significant

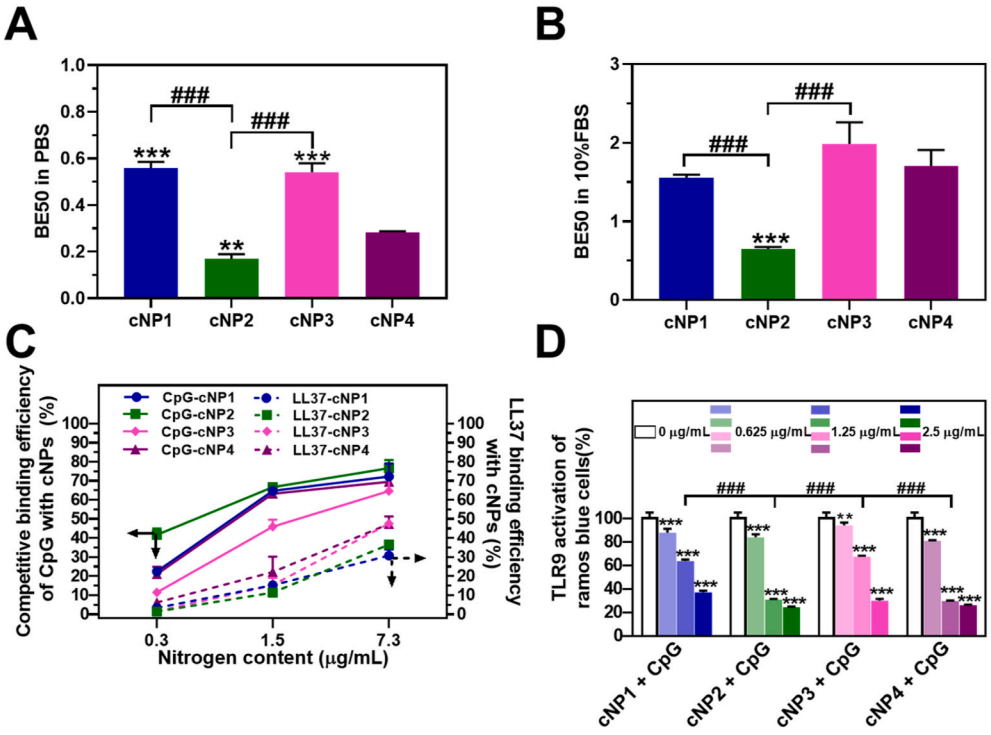

Fig. 2. Characterization of the DNA-binding ability and inhibition of TLR9 activation by cNPs. (A) N/P ratio resulting in 50% of cNPs-DNA binding (binding efficiency or BE) assessed by means of EtBr competition assay in PBS and (B) 10% FBS at 37 °C (n = 3; means ± SD; $^{**}0.001 < P < 0.01$, $^{***}P < 0.001$ versus cNP4; $\#\#\#P < 0.001$ between two groups). (C) Competitive binding efficiency of cNPs with CpG from the CpG-protein complex and protein binding efficiency with cNP1-cNP4 (n = 3; means ± SD). (D) Inhibition of TLR activation in Ramos Blue™ reporter cells using the QUANTI-Blue™ assay (n = 3; means ± SD). Statistical significance was calculated by one-way ANOVA with the LSD post-test, $^{**}0.001 < P < 0.01$, $^{***}P < 0.001$ versus 0 μg/mL materials + CpG. $\#\#\#P < 0.001$ between two groups.

inhibition of inflammation *in vitro*. To evaluate its therapeutic effects *in vivo*, CIA rats were randomly divided into four groups (n = 5) and intravenously injected with the four types of cNPs (the nitrogen content of the cNPs was kept equal to 1.69 mg/kg) and PBS, respectively. Healthy rats were used as negative control. The schedule of arthritis induction and treatment regimen was shown in Fig. 3A. After a single injection, all rats in the cNP4 group died, while the rats in the cNP1-cNP3 groups all survived, clearly suggesting that the cNPs with a hydroxyl shell had a better biocompatibility than cNP4, in agreement with the cellular cytotoxicity data. For the cNP1-cNP3 groups of rats, the arthritis severity was daily assessed by measuring the hind paws swelling volumes before the injections and ranked by the clinical score. As shown in Fig. 3B (i), the swelling volume of the hind paws rapidly increased from 1.5 mL to 3.3 mL in PBS-injected CIA rats due to disease progression, while almost no increase of swelling was observed for the hind paws of the rats in the cNP1 and cNP2 groups. The volume of the hind paws of the rats in the cNP3 group slightly increased from 1.5 mL to 1.8 mL. The more comprehensive clinical scoring system was applied to further evaluate the therapeutic efficacy of the cNPs. This evaluation system showed that cNP2 had the best therapeutic performance among the tested cNPs (Fig. 3B (ii)). A similar conclusion could be directly reached by analyzing the photographs of the hind paws of CIA rats treated with cNP1-cNP3 (Fig. 3C). Notably, the CIA rats in the cNP2 group showed no swelling, as in normal rats, while there was a significant swelling and a strong tendency to relapse for CIA rats treated with cNP3. In terms of forepaws, no incremental score was observed in all cNP-treated groups during the whole course (Fig. 3B (iii)).

The study of hematoxylin-eosin (H&E)-stained histological slides of the knees, ankles, digits, and wrists revealed the infiltration of inflammatory cells, pannus formation, and severe damage of bone and cartilage in PBS-treated CIA rats (Fig. 3D). Compared with the control, the pathological changes of arthritis were reduced in the CIA rats treated with cNP1-cNP3. Although cNP3 had a certain therapeutic effect and prevented cartilage erosion, there was still a significant infiltration of inflammatory cells. The rats in the cNP1 group showed a reduced inflammation damage in the joints, whereas the CIA rats treated with cNP2 exhibited the lowest histologic scores among the treatment groups. We also found that cNP2 could protect bone and cartilage from damage and restore the synovial area of the joints.

Consistently, we found that all cNPs could reduce the content of cfDNA in the synovia (Fig. 3E). The content of cfDNA in the inflamed knee joints significantly decreased from 6.1 μg/mL to 2.2 μg/mL in the cNP1 and cNP2 groups, while no significant decrease was found in the cNP3 group. It is remarkable to observe that the content of cfDNA in the cNP2-treated group was close to that of the normal group. We also measured the levels of pro-inflammatory cytokines (TNF-α, IL-6, and IL-1β) in the joints of CIA rats. For the model group, the levels of the three pro-inflammatory cytokines were highly elevated. In contrast, the treatment with cNP1-cNP3 led to a significant decline of TNF-α, IL-6, and IL-1β levels. Still, cNP2 outperformed cNP1 and cNP3, and the content of the three pro-inflammatory factors was 177 pg/mL, 761 pg/mL, and 459 pg/mL for TNF-α, IL-6, and IL-1β, respectively, which were close to the levels exhibited by the normal group. These data indicated that the treatment of CIA rats with cNP2 can significantly inhibit the progression of arthritis.

2.4. Biodistribution of cNPs in CIA rats

Although cNP1-cNP3 all carried hydroxyl groups to increase the biocompatibility, cNP2 showed the best therapeutic efficacy in the CIA rat model of arthritis. This result might be partly explained by considering the high affinity of cNP2 to cfDNA *in vitro*. The distribution of the nanoparticles *in vivo* could have been another key factor influencing their therapeutic effect. Thus, Near Infrared Fluorescence (NIRF) imaging was used to monitor AF750-labeled cNP1-cNP3 in CIA rats. As shown in Fig. 4A, the fluorescence intensity of the forepaw and hind joints was different in treated CIA rats with the order cNP2>cNP1>cNP3. The *ex vivo* NIRF images of the main organs and joints showed a similar trend of fluorescence distribution (Fig. 4B and C). At 48 h, the liver and kidneys of rats in the cNP3 group showed a lower fluorescence signal than the organs of rats in the cNP1 and cNP2 groups, suggesting that cNP3 might be cleared by renal excretion more rapidly than cNP1 and cNP2. Notably, the animals in the cNP2 group showed a stronger fluorescence intensity in paw joints and extracted organs, whereas the fluorescence significantly decreased in rats treated with cNP3, demonstrating that cNP2 had the longest blood circulation time among the tested cNPs.

2.5. Systemic toxicity of cNPs in CIA rats

Next, since the potential toxicity of cNPs is a major obstacle to their use for the treatment of RA *via* cfDNA scavenging, we assessed if the presence of the hydroxyl shell alleviates the cNP toxicity. As we have previously described, the CIA rats died the day after the first injection with cNP4 at the dose of 1.69 mg/kg. Conversely, the animals survived when treated with cNP1-cNP3 at the same equivalent nitrogen dose (Fig. 5A), suggesting that the systemic toxicity of cNP1-cNP3 was significantly reduced by the addition of the flanking hydroxyl groups. We also assessed the changes in the biochemical indexes in CIA rats after 15 days of a single intravenous treatment with cNP1-cNP3. The levels of ALP, ALT, AST, creatinine, urea, and uric acid in the rats of the cNP1-cNP3 groups were within the normal range (Fig. 5B), indicating that the nanoparticles had no side effects on the liver and renal functions of CIA rats. Additionally, H&E-stained histologic slides of the CIA rats' organs (Fig. 5C) showed that the main organs (heart, liver, spleen, lung, and kidney) did not display any significant damage.

Taken together, our results suggested that the better therapeutic efficacy of cNP2 respect with the other tested cNPs was due to a combination of a greater affinity to cfDNA in the presence of a protein corona and more favorable pharmacokinetic and biocompatibility profiles and joint retention time.

2.6. Assessment of the cNPs' protein corona

Finally, we assess the protein corona formed on the cNPs' surface to shed light on the possible biologic mechanisms modulating how the chemical properties of cNPs affect their biodistribution and biocompatibility profiles and therapeutic efficacy. The ability to resist protein attachment is highly required for polycationic scavengers. To prove this point, BSA was used as a model protein to simulate the interaction between cNPs and proteins *in vivo*. Fig. S8 showed the results of the protein adsorption assays. After 1 h of incubation of cNPs with BSA at physiological pH, ~1 mg/mg of BSA adsorbed onto cNP4 and the solution turned from clear to milky white (Fig. S9). Conversely, much less BSA adsorbed onto cNP2 (Figs. S8 and S9). The superior ability of cNP2 to resist BSA adsorption was attributed to the hydroxyl groups flanking the amino group, which might explain the greater stability in blood and cfDNA scavenging efficiency of cNP2 respect with the other tested cNPs.

To further characterize the cNPs' protein corona, cNP1-cNP4 were incubated in either 80% fetal bovine serum (FBS) or rat plasma for 1 h, respectively. Then, 10% sodium dodecyl sulfate (SDS) was used to remove the adsorbed proteins and the isolated proteins were separated by 1D gel electrophoresis. The 1D gel electrophoresis showed that the amount of proteins in the coronas of cNP3 and cNP4 were higher than that of cNP1 and cNP2 (Figs. S10 and S11). Furthermore, label-free quantitative technique (LFQ) was used to identify and quantify protein corona on cNPs. Proteomic analysis showed that the plasma proteins with a 30–60 kDa molecular weight constituted the majority of the adsorbed proteins (Fig. 6A) and the proteins bearing a net negative charge (pI < 7) were significantly enriched in all cNPs' protein corona, irrespective of the type of nanoparticle (Fig. 6B).

Then, we divided the isolated proteins into different groups

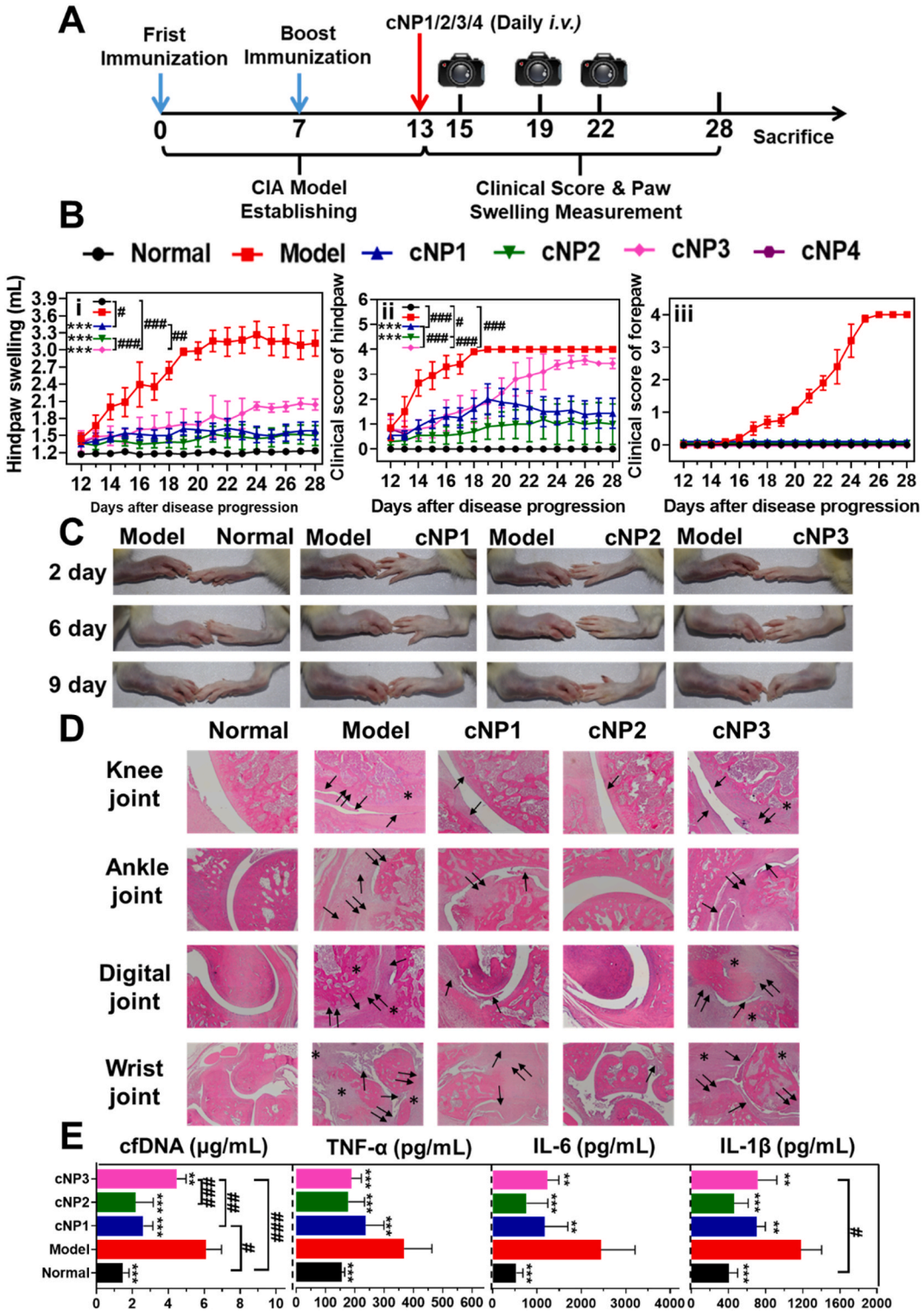

Fig. 3. Therapeutic efficacy of cNPs in CIA rats. (A) Experimental schedule of the CIA model rats. After immunization with collagen type II and Freund's adjuvant twice (at day 0 and day 7), the CIA model was developed in rats. Then CIA rats were intravenously injected with cNP1-cNP3 from day 13 to day 28. Photos were taken regularly during therapy. Further study was performed after the rats were sacrificed on day 28. (B) (B-i) Volume change of hind paws, clinical scores of the (B-ii) hind paws, and (B-iii) forepaws of CIA rats. n = 5 for each group. Data are presented as the mean ± SD. (C) Photographs of hind paws swelling of cNP1-cNP3 treatment groups at day 15 (treatment for 2 days), day 19 (treatment for 6 days), and day 22 (treatment for 9 days). (D) Histological analysis with H&E staining of the knee, ankle, digital, and wrist joints of cNP1-cNP3 treatment groups at day 28 (× 200). The single arrows indicate inflammatory cell infiltration in the synovium, double arrows indicate the erosion of cartilage, and the asterisks indicate bone erosion. (E) The levels of cfDNA and pro-inflammatory cytokines (TNF-α, IL-1β, and IL-6) in knee joints of cNP1-cNP3 treatment groups at day 28. Statistical significance was calculated by one-way ANOVA with the LSD post-test, ** $0.001 < P < 0.01$, ***$P < 0.001$ versus model. # $0.01 < P < 0.05$, ## $0.001 < P < 0.01$, ###$P < 0.001$ between two groups. Data are presented as the mean ± SD.

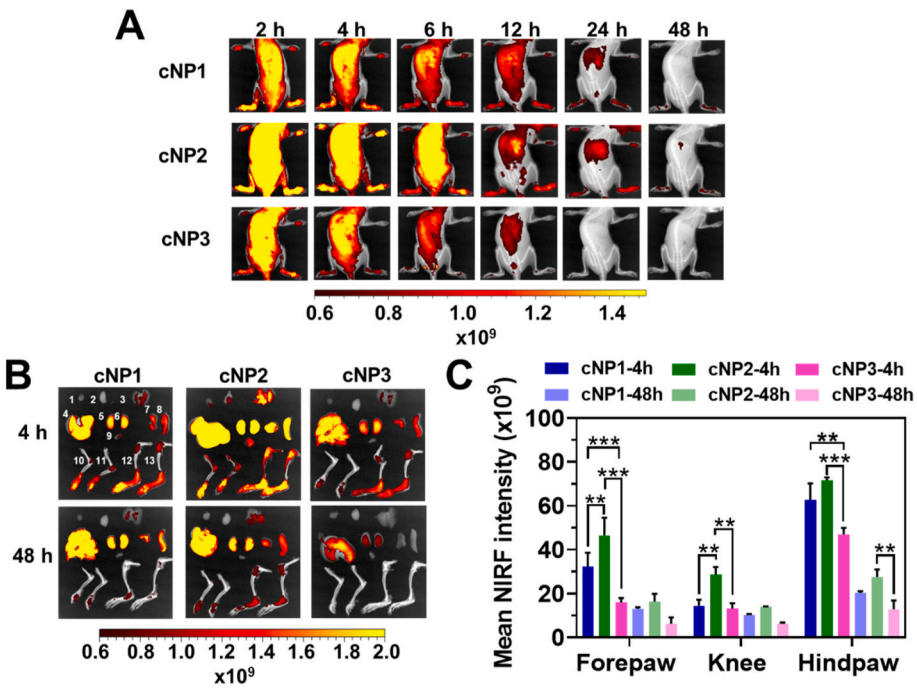

Fig. 4. Biodistribution of cNPs in CIA rats. (A) *In vivo* and (B) *ex vivo* near-infrared fluorescence (NIRF) imaging of CIA rats at various time points after intravenous treatment with cNP1-cNP3. Legend: (1) thymus; (2) heart; (3) lung; (4) liver; (5) and (6) kidneys; (7) pancreas; (8) spleen; (9) bladder; (10) and (11) forelimbs; (12) and (13) hind limbs. (C) Average percentage of cNPs in forepaws, knees, and the hind paws of CIA rats were calculated by NIRF intensity (n = 3, means ± SD). Statistical significance was calculated by one-way ANOVA with the LSD post-test, $^{**}0.001 < P < 0.01$, $^{***}P < 0.001$.

according to their physiological functions and displayed the quantity of proteins contained in each group (Fig. 6C and Fig. S12). This analysis showed that the differences in the composition of the cNPs' protein corona were driven by a combination of the nanoparticles' surface functional groups and the proteins' physiological function. Apolipoprotein was the most abundant plasma proteins in the protein corona of all the tested cNPs, whereas the complement proteins were found in high abundance in the protein corona of cNP1 and cNP3. The protein corona of cNP1 showed a high abundance of coagulation proteins and tissue leakage proteins, while the corona of cNP3 showed a high abundance of acute phase proteins (Fig. 6C). We further identified and semi-quantitatively analyzed the 20 most abundant proteins among the approximately 100 different of proteins isolated from the corona of cNP1-cNP4. The results were summarized in a heat map in Fig. 6D. The heat map showed several aspects of the cNPs' protein corona. Notably, the coronas of all four cNPs contained relatively small amounts of serum albumin (10% or less) which is the most abundant protein in plasma (more than 50%) [34,35]. As serum albumin has a structure similar to surfactants (hydrophobic core and hydrophilic shell), serum albumin is considered to be more stable in water than on the cNPs' surface [30]. Therefore, the serum albumin content in the cNPs' protein corona was much less than that in plasma. Macroglobulin, the second most abundant plasma protein [35], was only the 7–11th most abundant protein detectable on the corona of cNP1-cNP3. Instead, the cNPs' protein corona contained proteins that are not abundant in plasma, for example, complement C3 and C4 which play the major role in the opsonization process. Vitronectin, a multifunctional adhesive glycoprotein [36], had high affinity with the positively charged cNPs [37], and it was enriched in the protein corona of the cNPs we tested. Another plasma protein highly enriched in the cNPs' protein corona was apolipoprotein (15% or above) which associates with lipid and cholesterol transport and metabolism [29]. Particularly, apolipoprotein E, A-I and B-100 were also enriched in the cNPs' protein corona. In addition to the high quantity of apolipoproteins, vitronectin, serum albumin, complement proteins and macroglobulin on the surface of all four cNPs, the amount of other abundant proteins was different for each type of particle (Table S3). These findings illustrated that cNP1-cNP3 decorated with a hydroxyl shell and different types of amino groups showed different selectivity for the proteins in rat plasma, as shown by the composition of their protein corona (Table S4).

3. Discussion

In this work, we successfully synthesized hydroxyl-rich polycationic PCL_{60}-*b*-PGDMEN/EA/EDA_{150} by post-modification with different amines on PCL_{60}-*b*-$PGMA_{150}$. Then, cNPs with a hydroxyl shell were fabricated by self-assembly of PCL_{60}-*b*-PGDMEN/EA/EDA_{150} and used as cfDNA scavengers. Except for the different amine species (primary, secondary and tertiary amines), all the fabricated cNPs had a hydroxyl shell, which eventually decreased the side-effects to both cells and CIA rats without decreasing the ability to scavenge cfDNA. Protein adsorption assay and proteomic analysis were carried out to demonstrate that the cNPs decorated with a hydroxyl shell could reduce the adsorption of a protein corona in comparison with the non-hydroxylated nanoparticles. Moreover, we found that the protein corona of the fabricated cNPs were enriched in apolipoproteins and immunoglobulins, as well as complement, acute phase, tissue leakage and coagulation proteins (Fig. 6C and Fig. S12A). Apolipoproteins accounted for ~20% of the total proteins in the cNPs' corona. The amphiphilic characteristics of apolipoproteins enabled them to firmly adhere to the surface of cNPs and possibly form a hard corona. Particularly, apolipoprotein E, A-I and B-100, members of the dysopsonin family, were the three kinds of apolipoproteins with the most abundance in the cNPs' protein corona (Fig. S12B). These apolipoproteins have been reported to facilitate the entry of NPs into endothelial cells [38–40]. In contrast, it has been reported that the presence of β-2-glycoprotein (Apo H) in the protein corona may play a role in the clearance of NPs by phagocytic cells of the reticuloendothelial system (RES) [41,42]. We found that Apo H was ~2.4 times more enriched in the corona of cNP1 than cNP2 (Table S4). Immunoglobulins (Ig) are globular glycoproteins with antibody activity. As important immune effector molecules, Ig play a critical role in the activation of the immune system and induce phagocytosis. According to the amino acid sequences of the heavy chain region, Ig could be divided into five categories, namely IgG, IgA, IgM, IgD and IgE [42]. IgM accounted for 50% of the immunoglobulin component of the protein corona of cNP1-cNP4 (Fig. S12C), and the fractions of IgM in the protein corona of cNP1, cNP3 and cNP4 were ~1.1, ~1.4 and ~1.5 times, respectively, higher than that of cNP2 (Table S4). In addition to Ig,

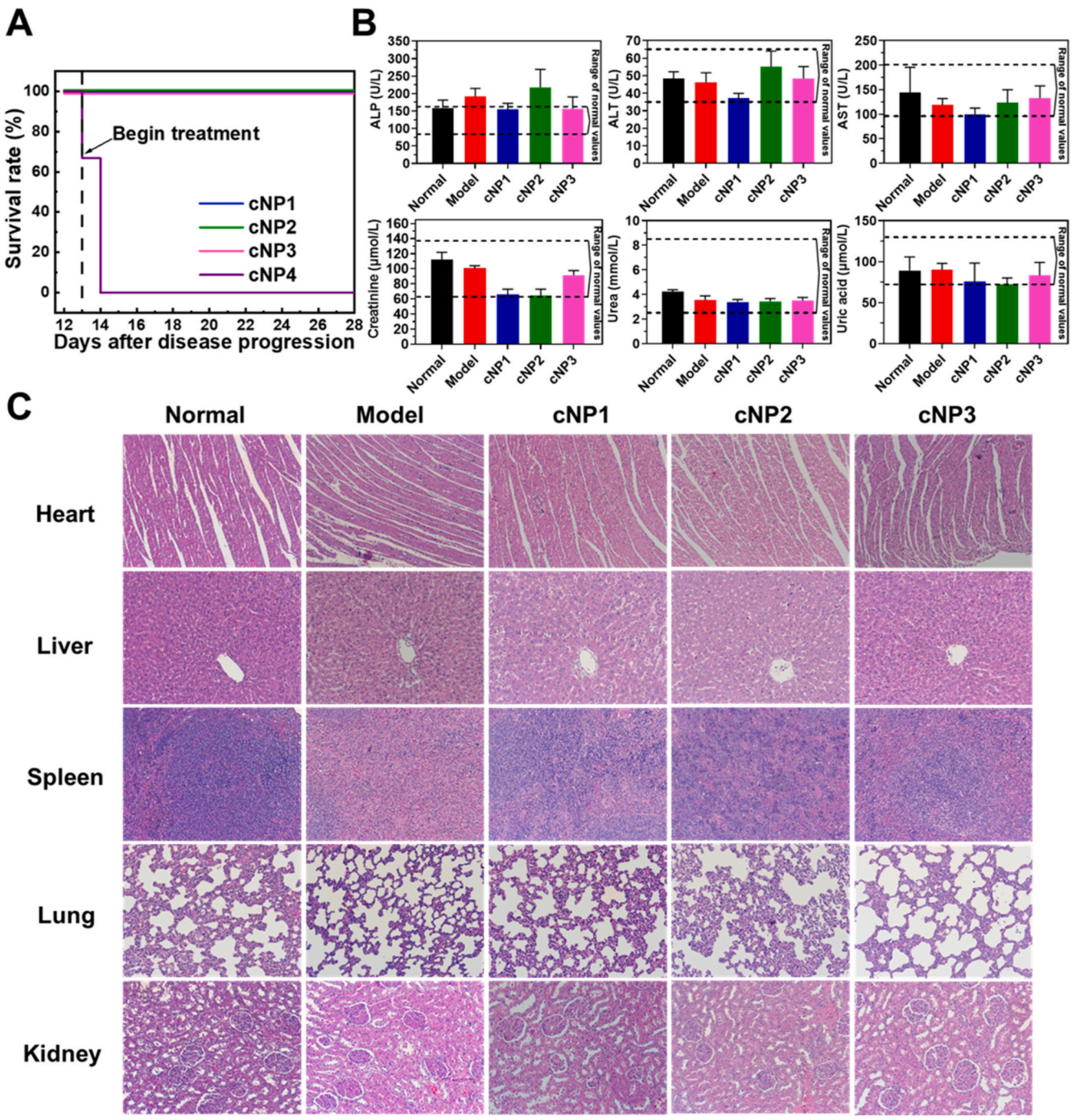

Fig. 5. Toxicity of cNPs in CIA rats. (A) Survival curves of rats treated with cNP1-cNP4. The initial number of rats was 5 for each group. (B) ALP, ALT, AST, creatinine, urea, and uric acid analysis of CIA rats at day 28 (treatment for 15 days). The normal ranges of ALP, ALT, and AST are 84–162, 34.6–64.0 and 96–200 U/L, respectively. The normal ranges of creatinine, uric acid, and urea levels in rat serum are 63.5–137.1 μmol/L, 71.4–133.3 μmol/L and 3.33–8.33 mmol/L, respectively. Data were presented as the mean ± SD. (C) H&E staining of heart, liver, spleen, lung, and kidney samples extracted from normal, PBS-treated and cNP-treated rats (× 200).

complement proteins also play an important role in the activation of the immune system. The lowest fractional binding of complement proteins (C3, C4, C4b, C7, C8 and C9) was found for the protein corona of cNP2 compared with those of cNP1 and cNP3 (Fig. S12 D, Table S4). Fibrinogen (HFG) is a coagulation protein and is associated with inflammation. The content of HFG in the protein corona of cNP3 and cNP2 showed no significant difference, but it was ~2.1 and ~1.4 times lower than that in the protein corona of cNP1 and cNP4, respectively (Fig. S12 G, Table S4). Overall, the above data indicated that the introduction of a hydroxyl shell could assist in reducing the adsorption of those opsonins (ApoH, IgM, complement proteins and HFG) which negatively affect the bioavailability of cNPs, while negligibly affecting the inhibition of dysopsonins (apolipoprotein E and serum albumin) playing a protective role. Furthermore, the individually distinct protein corona could influence the transport, retention, and phagocytosis of cNPs, guiding their fate in the body. Also, the adsorption of proteins with a critical role in the activation of the immune response may affect the efficacy of cNPs as a novel RA treatment *via* cfDNA scavenging, as it has been described in

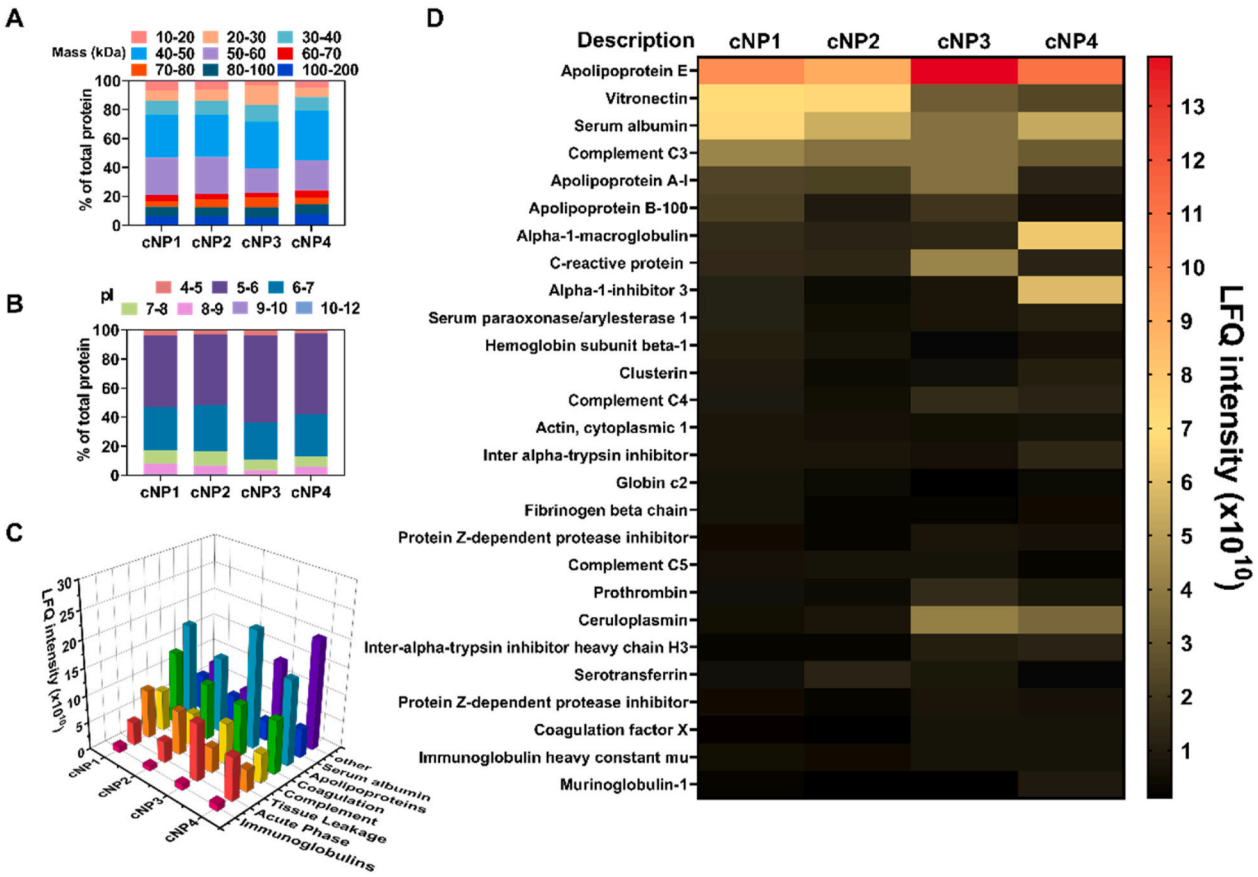

Fig. 6. Protein corona of cNPs. Classification of surface-bound proteins after 1 h incubation of cNPs in 80% rat plasma according to their (A) molecular weight and (B) calculated isoelectric point (pI). (C) Classification of identified proteins in the corona of cNP1-cNP4 according to their physiological functions. (D) Heat map of the most abundant proteins in the protein corona of cNP1-cNP4 after 1 h incubation in 80% rat plasma determined by proteomic mass spectrometry. Values were calculated from the LFQ intensity of each protein identified by LC-MS. Only the top 20 most-abundant proteins in the corona of cNP1-cNP4 were shown in the heat map.

this work.

4. Conclusions

In this work, we focused on the development of safe cationic materials to neutralize cfDNA, which is a causative agent for RA. We fabricated cNPs with a hydroxyl shell and they showed excellent serum tolerance and biocompatibility. Remarkably, the introduction of a hydroxyl shell did not affect the DNA binding affinity and the potent therapeutic efficacy to CIA rat models of the nanoparticles. The introduction of a hydroxyl shell also reduced the adsorption of proteins onto the cNPs' surface and, thus prolonged the circulation and site accumulation of the nanoparticles. Our data showed that the composition of the protein corona formed onto the cNPs in the serum can be modulated by their synthetic identity, and, in turn, affect the fate and functions of the cNPs. This work shed light on a novel approach for the preparation of safe polycationic DNA scavengers.

5. Experimental section

5.1. Synthesis of PCL_{60}-b-$PGMA_{150}$

PCL_{60}-*b*-$PGMA_{150}$ was prepared *via* atom transfer radical polymerization (ATRP) of glycidyl methacrylate (GMA) in dry anisole using the macroinitiator PCL_{60}-Br. In a typical polymerization, GMA (5 g, 35.2 mmol), CuCl (23.23 mg, 0.23 mmol), PCL_{60}-Br (1.6 mg, 0.23 mol), 2,2-bispyridine (bpy) (71.85 mg, 0.46 mmol) and 6 mL dry anisole were introduced to a dry Schlenk tube equipped with a magnetic stir bar. The mixture was deoxygenated by three freeze-pump-thaw cycles, then the polymerization was carried out in a thermostatic oil bath at 50 °C for 24 h. The polymerization was terminated by freezing the reaction mixture with liquid N_2 and exposing to air. The reaction mixture was diluted with THF and passed through neutral alumina to remove the catalyst as much as possible and then rotary evaporated to eliminate the solvent. The solution was poured into a large excess of cold ether. Finally, the polymers were dried under a vacuum for 24 h. The degree of polymerization of GMA was determined to be ~150 by comparing the areas of the peaks corresponding to methylene protons (-COOC***H***$_2$-epoxy, 4.30, 3.80 ppm) in GMA block and methylene protons (-COOC***H***$_2$$(CH_2)_4$OOC-, 2.30 ppm) of PCL in the ^{1}H NMR spectrum (Fig. S3 C). Yield: 85%. ^{1}H NMR (400 MHz, $CDCl_3$, δ, ppm, Fig. S3 C): 7.30–7.38 (m, 5H, ***Ar***), 5.11 (s, 2H, Ar-C***H***$_2$-), 4.30 (s, 1H, -COOC***H***$_2$-epoxy) 4.05 (t, 2H, –$COOCH_2CH_2CH_2CH_2C$***H***$_2$OOC-), 3.80 (s, 1H, -COOC***H***$_2$-epoxy), 3.22 (s, 1H, -epoxy), 2.83 (s, 1H, -epoxy), 2.63 (s, 1H, -epoxy), 2.30 (t, 2H, -COOC***H***$_2$$CH_2CH_2CH_2CH_2$OOC-), 1.89 (m, 2H, the backbone of PGMA) 1.64 (m, 4H, –$COOCH_2C$***H***$_2$$CH_2C$***H***$_2$$CH_2$OOC-), 1.37 (m, 2H, –$COOCH_2CH_2C$***H***$_2$$CH_2CH_2$OOC-), 0.93–1.08 (d, 3H, the backbone of PGMA). The molecular weights of PCL_{60}-*b*-$PGMA_{150}$ was summarized in Table S1.

5.2. Synthesis of PCL_{60}-b-$PGDMEN/EA_{150}$

For preparation of PCL_{60}-*b*-$PGDMEN/EA_{150}$, 0.5 g of PCL_{60}-*b*-$PGMA_{150}$ was dissolved in 14 mL of DMSO. 5 mL of N,N-dimethyl ethylenediamine for PCL_{60}-*b*-$PGDMEN_{150}$ and ethanol amine for PCL_{60}-*b*-$PGEA_{150}$ were then added. The reaction mixture was stirred at 80 °C for

4 h to produce PCL_{60}-*b*-PGDMEN/EA_{150}. The final reaction mixture was precipitated and washed with excess diethyl ether, prior to be redissolved in 15 mL of deionized water and dialyzed against deionized water with dialysis membrane (MWCO, 3500 Da) at room temperature for 24 h. The final products were freeze-dried. Yield: 90%.

5.3. Synthesis of PCL_{60}-b-$PGEDA_{150}$

The PCL_{60}-*b*-$PGEDA_{150}$ was synthesized *via* ring-opening polymerization of PCL_{60}-*b*-$PGMA_{150}$ using the N-Boc-ethylenediamine as a monomer, followed by de-protection of the Boc group in the presence of trifluoroacetic acid. In briefly, 0.5 g of PCL_{60}-*b*-$PGMA_{150}$ was dissolved in 14 mL of DMSO. 5 mL of N-Boc-ethylenediamine were then added. The reaction mixture was stirred at 80 °C for 4 h to produce PCL_{60}-*b*-$PGEDA_{150}$-Boc. The solution was poured into a large excess of cold ether. Finally, the polymers were dried under a vacuum for 24 h. Yield: 80%.

In the second step, 0.5 g PCL_{60}-*b*-$PGEDA_{150}$-Boc was dissolved in 5 mL DCM containing 5 mL trifluoroacetic acid and the solution was stirred at room temperature for 12 h. Next, a 10-fold excess of diethyl ether (30 mL) was added to precipitate the polymer. The precipitated crude was dissolved in distilled water and dialyzed against deionized water with dialysis membrane (MWCO, 3500 Da). The PCL_{60}-*b*-$PGEDA_{150}$ was then obtained as white powder after lyophilization. In the ^{1}H NMR spectrum shown in Fig. S5 C, the signal at 1.37 ppm disappeared, indicating the complete hydrolysis of Boc groups of PCL_{60}-*b*-$PGEDA_{150}$-Boc. Yield: 80%.

5.4. Preparation of cNP1-cNP4

PCL_{60}-*b*-PGDMEN/EA/EDA_{150} and PCL_{60}-*b*-$PDMA_{150}$ (20 mg) was dissolved in 1 mL of DMF, respectively. The origin solution was added dropwise into 9 mL PBS (pH = 7.4) under ultrasound (Sonics VCX105, 20 kHz, 70% power level) in an ice bath. The final solution was dialyzed against PBS (pH = 7.4) to remove DMF. The cNP1-cNP4 were characterized by dynamic light scattering (DLS), transmission electron microscopy (TEM), and Zeta-Nanosizer as described in instrumentation.

5.5. Cell assays

Cytotoxicity of cNP1-cNP4 was evaluated using the MTT assay in RAW 264.7 cells. The inhibition of TLR9 by cNP1-cNP4 was conducted in Ramos Blue™ reporter cell, CpG OND 2006 was used as the extracellular agonist. The details for these assays were provided in Supporting Information.

5.6. Protein adsorption assay

In brief, 1 mL of cNP1-cNP4 (1 mg/mL) was added to 1 mL BSA solution (2 mg/mL). After shaking at 37 °C for 1 h and following centrifugation, the upper layer was carefully collected. The concentration of BSA in the supernatant was determined from the UV absorbance (280 nm), using a calibration curve obtained from BSA solutions of known concentrations. Thus, the protein adsorbed on the cNPs was calculated by $(C_i\text{-}C_s)V/m$, where C_i was the initial BSA concentration, C_s was the BSA concentration of supernatant after adsorption experiments, V was the volume of the solution (2 mL), and m was the weight of the cNPs (1 mg).

5.7. Incubation with rat plasma or FBS

cNP1-cNP4 (50 μg) were incubated for 1 h at 37 °C with 400 μL of rat plasma or FBS in a final volume of 500 μL by adding PBS (80% final plasma or FBS concentration). The samples were washed four times in 1 mL of PBS by ultracentrifugation at 12,000 g at 4 °C for 30 min, then the final pellets were resuspended in loading buffer and boiled at 98 °C for 5 min. After 5 min of ultrasonic dispersion, the solutions were run on a 20% SDS-PAGE gel and stained with Coomassie brilliant blue.

5.8. In-gel digestion and sample preparation for LC-MS/MS analysis

Stained SDS-PAGE bands were cut into 2 mm^3 pieces, transferred to an Eppendorf tube, destained by washing with decolorizing agent (the ratio of acetonitrile (ACN) and 50 mM NH_4HCO_3 is 66.7%), and vacuum-dried. Proteins were reduced with 10 mM dithiothreitol (10 μL 1 M DTT, 990 μL 25 mM NH_4HCO_3) at 56 °C for 45 min and alkylated with 15 mM iodoacetamide (22 μL 1 M IAM, 378 μL 25 mM NH_4HCO_3) in the dark for 15 min prior digestion by 5 ng/μL trypsin in 25 mM NH_4HCO_3 for 5 min on ice followed by additional 12 h at 37 °C. The reaction was terminated by adding 5% formic acid (FA), and the pH < 4 (FA final concentration was 0.2%–0.5%), then centrifuged.

5.9. Protein identification using LC/MS/MS

LC-MS/MS assays were conducted on nanoLC-Q EXACTIVE (Thermo Scientific). The digested peptides were separated by a C18 reverse phase column (75 μm × 20 cm, 3 μm). The solvent A, 0.1% formic acid (FA) in 100% water solution and the solvent B, 0.1% FA in 100% acetonitrile solution. The gradient was set as 4–8% B, 0–8 min; 8–22% B, 8–58 min; 22–32%, B, 58–70 min; 32–90% B, 70–71 min; 90% B, 71–78 min. The flow rate was 300 nL/min.

The purified peptides were analyzed on nanoLC-Q Exactive mass spectrometer (Thermo Scientific). The electrospray voltage was 2.0 kV and the capillary temperature was 320 °C. The dynamic exclusion time was 40 s. The MS data were obtained in the mass range of 300–1600 *m/z*. The data collection mode is 1–20 (that is, a complete MS1 scan followed by a second-order spectrum MS2 analysis of 20 highest abundance ions).

The raw data were analyzed by using Thermo Proteome Discoverer (version 2.2.0.388) with SEQUEST HT search engine for peptide identification against Uniprot-proteom-rat (update-20171,001). When searching, trypsin was selected as enzyme and two missed cleavages were set; the mass error of precursor ions was less than 10 ppm and the mass error of fragment ions was less than 20 mDa. Percolator was used to filter the spectrum, Delta CN was less than 0.1, FDR was set as 1%, Peptide confidence was selected as High as the filtering parameter, and FDR of protein level was also set as 1%.

5.10. Statistical analysis

Experiment data were presented as the mean ± standard deviation (SD), and Statistical significance was calculated by one-way ANOVA with the LSD post-test, $*0.01 < P < 0.05$, $**0.001 < P < 0.01$, $***P < 0.001$.

CRediT authorship contribution statement

Xingliang Liu: Investigation, Methodology, Writing – original draft. **Huiyi Liang:** Methodology. **Yanzi Yan:** Methodology. **Jingjiao Wu:** Methodology. **Massimo Bottini:** Writing – review & editing, Validation. **Lixin Liu:** Supervision, Writing – review & editing, Funding acquisition. **Yongming Chen:** Supervision, Writing – review & editing, Funding acquisition.

Declaration of competing interest

The authors declare no conflict of interest.

Acknowledgments

The financial support from the National Natural Science Foundation of China (21875290), the key Areas Research and Development Program of Guangzhou (202007020006) and support of Sun Yat-sen University

(19lgjc01) was acknowledged for support.

Appendix A. Supplementary data

Supplementary data to this article can be found online at https://doi.org/10.1016/j.bioactmat.2021.10.044.

References

[1] M. Jeong, J.H. Park, Nanomedicine for the treatment of rheumatoid arthritis, Mol. Pharm. 18 (2021) 539–549.
[2] I.M. Oliveira, C. Gonçalves, R.L. Reis, J.M. Oliveira, Engineering nanoparticles for targeting rheumatoid arthritis: past, present, and future trends, Nano Res 11 (2018) 4489–4506.
[3] J.S. Smolen, D. Aletaha, I.B. McInnes, Rheumatoid arthritis, Lancet 388 (2016) 2023–2038.
[4] G.R. Burmester, J.E. Pope, Novel treatment strategies in rheumatoid arthritis, Lancet 389 (2017) 2338–2348.
[5] S. Dolati, S. Sadreddini, D. Rostamzadeh, M. Ahmadi, F. Jadidi-Niaragh, M. Yousefi, Utilization of nanoparticle technology in rheumatoid arthritis treatment, Biomed, Pharma 80 (2016) 30–41.
[6] Q. Wang, X. Sun, Recent advances in nanomedicines for the treatment of rheumatoid arthritis, Biomater. Sci. 5 (2017) 1407–1420.
[7] Y. Madav, K. Barve, B. Prabhakar, Current trends in theranostics for rheumatoid arthritis, Eur. J. Pharmaceut. Sci. 145 (2020) 105240.
[8] B. Duvvuri, C. Lood, Cell-free DNA as a biomarker in autoimmune rheumatic diseases, Front. Immunol. 10 (2019).
[9] X.Y. Zhong, I. von Mühlenen, Y. Li, A. Kang, A.K. Gupta, A. Tyndall, W. Holzgreve, S. Hahn, P. Hasler, Increased concentrations of antibody-bound circulatory cell-free DNA in rheumatoid arthritis, Clin. Chem. 53 (2007) 1609–1614.
[10] D.S. Pisetsky, J. Gauley, A.J. Ullal, Microparticles as a source of extracellular DNA, Immunol. Res. 49 (2011) 227–234.
[11] A.F. Orozco, C.J. Jorgez, C. Horne, D.A. Marquez-Do, M.R. Chapman, J.R. Rodgers, F.Z. Bischoff, D.E. Lewis, Membrane protected apoptotic trophoblast microparticles contain nucleic acids: relevance to preeclampsia, Am. J. Pathol. 173 (2008) 1595–1608.
[12] T. Hashimoto, K. Yoshida, N. Hashimoto, A. Nakai, K. Kaneshiro, K. Suzuki, Y. Kawasaki, N. Shibanuma, A. Hashiramoto, Circulating cell free DNA: a marker to predict the therapeutic response for biological DMARDs in rheumatoid arthritis, Int. J. Rheum. Dis. 20 (2017) 722–730.
[13] C. Dong, Y. Liu, C. Sun, H. Liang, L. Dai, J. Shen, S. Wei, S. Guo, K.W. Leong, Y. Chen, L. Wei, L. Liu, Identification of specific joint-inflammatogenic cell-free DNA molecules from synovial fluids of patients with rheumatoid arthritis, Front. Immunol. 11 (2020).
[14] J. Lee, J.W. Sohn, Y. Zhang, K.W. Leong, D. Pisetsky, B.A. Sullenger, Nucleic acid-binding polymers as anti-inflammatory agents, Proc. Natl. Acad. Sci. Unit. States Am. 108 (2011) 14055–14060.
[15] H. Yanai, T. Ban, Z. Wang, M.K. Choi, T. Kawamura, H. Negishi, M. Nakasato, Y. Lu, S. Hangai, R. Koshiba, D. Savitsky, L. Ronfani, S. Akira, M.E. Bianchi, K. Honda, T. Tamura, T. Kodama, T. Taniguchi, HMGB proteins function as universal sentinels for nucleic-acid-mediated innate immune responses, Nature 462 (2009) 99–103.
[16] R. Lande, J. Gregorio, V. Facchinetti, B. Chatterjee, Y.H. Wang, B. Homey, W. Cao, Y.H. Wang, B. Su, F.O. Nestle, T. Zal, I. Mellman, J.M. Schröder, Y.J. Liu, M. Gilliet, Plasmacytoid dendritic cells sense self-DNA coupled with antimicrobial peptide, Nature 449 (2007) 564–569.
[17] V. Urbonaviciute, B.G. Fürnrohr, S. Meister, L. Munoz, P. Heyder, F. De Marchis, M. E. Bianchi, C. Kirschning, H. Wagner, A.A. Manfredi, J.R. Kalden, G. Schett, P. Rovere-Querini, M. Herrmann, R.E. Voll, Induction of inflammatory and immune responses by HMGB1–nucleosome complexes: implications for the pathogenesis of SLE, J. Exp. Med. 205 (2008) 3007–3018.
[18] J. Tian, A.M. Avalos, S.Y. Mao, B. Chen, K. Senthil, H. Wu, P. Parroche, S. Drabic, D. Golenbock, C. Sirois, J. Hua, L.L. An, L. Audoly, G. La Rosa, A. Bierhaus, P. Naworth, A. Marshak-Rothstein, M.K. Crow, K.A. Fitzgerald, E. Latz, P.A. Kiener, A.J. Coyle, Toll-like receptor 9–dependent activation by DNA-containing immune complexes is mediated by HMGB1 and RAGE, Nat. Immunol. 8 (2007) 487–496.
[19] M. Dunaeva, B.C. Buddingh', R.E.M. Toes, J.J. Luime, E. Lubberts, G.J.M. Pruijn, Decreased serum cell-free DNA levels in rheumatoid arthritis, Autoimmun. Highlights 6 (2015) 23–30.
[20] P. Jiang, Y.M.D. Lo, The long and short of circulating cell-free DNA and the ins and outs of molecular diagnostics, Trends Genet. 32 (2016) 360–371.
[21] C.M. Lau, C. Broughton, A.S. Tabor, S. Akira, R.A. Flavell, M.J. Mamula, S. R. Christensen, M.J. Shlomchik, G.A. Viglianti, I.R. Rifkin, A. Marshak-Rothstein, RNA-associated autoantigens activate B cells by combined B cell antigen receptor/Toll-like receptor 7 engagement, J. Exp. Med. 202 (2005) 1171–1177.
[22] E.K. Holl, K.L. Shumansky, L.B. Borst, A.D. Burnette, C.J. Sample, E.A. Ramsburg, B.A. Sullenger, Scavenging nucleic acid debris to combat autoimmunity and infectious disease, Proc. Natl. Acad. Sci. Unit. States Am. 113 (2016) 9728–9733.
[23] J. Dawulieti, M. Sun, Y. Zhao, D. Shao, H. Yan, Y.H. Lao, H. Hu, L. Cui, X. Lv, F. Liu, C.W. Chi, Y. Zhang, M. Li, M. Zhang, H. Tian, X. Chen, K.W. Leong, L. Chen, Treatment of severe sepsis with nanoparticulate cell-free DNA scavengers, Sci. Adv. 6 (2020) 7148.
[24] H. Liang, Y. Yan, J. Wu, X. Ge, L. Wei, L. Liu, Y. Chen, Topical nanoparticles interfering with the DNA-LL37 complex to alleviate psoriatic inflammation in mice and monkeys, Sci. Adv. 6 (2020) 5274.
[25] H. Liang, B. Peng, C. Dong, L. Liu, J. Mao, S. Wei, X. Wang, H. Xu, J. Shen, H. Q. Mao, X. Gao, K.W. Leong, Y. Chen, Cationic nanoparticle as an inhibitor of cell-free DNA-induced inflammation, Nat. Commun. 9 (2018) 4291.
[26] B. Peng, H. Liang, Y. Li, C. Dong, J. Shen, H.-Q. Mao, K. Leong, Y. Chen, L. Liu, Tuned cationic dendronized polymer as a molecular scavenger for rheumatoid arthritis treatment, Angew. Chem. 131 (2019).
[27] J. Wu, H. Liang, Y. Li, Y. Shi, M. Bottini, Y. Chen, L. Liu, Cationic block copolymer nanoparticles with tunable DNA affinity for treating rheumatoid arthritis, Adv. Funct. Mater. 30 (2020) 2000391.
[28] V.H. Nguyen, B.-J. Lee, Protein corona: a new approach for nanomedicine design, Int. J. Nanomed. 12 (2017) 3137–3151.
[29] S. Tenzer, D. Docter, J. Kuharev, A. Musyanovych, V. Fetz, R. Hecht, F. Schlenk, D. Fischer, K. Kiouptsi, C. Reinhardt, K. Landfester, H. Schild, M. Maskos, S. K. Knauer, R.H. Stauber, Rapid formation of plasma protein corona critically affects nanoparticle pathophysiology, Nat. Nanotechnol. 8 (2013) 772–781.
[30] Y. Zou, S. Ito, F. Yoshino, Y. Suzuki, L. Zhao, N. Komatsu, Polyglycerol grafting shields nanoparticles from protein corona formation to avoid macrophage uptake, ACS Nano 14 (2020) 7216–7226.
[31] Q.F. Zhang, W.J. Yi, B. Wang, J. Zhang, L. Ren, Q.M. Chen, L. Guo, X.Q. Yu, Linear polycations by ring-opening polymerization as non-viral gene delivery vectors, Biomaterials 34 (2013) 5391–5401.
[32] R.Q. Li, Y. Wu, Y. Zhi, X. Yang, Y. Li, F.J. Xu, J. Du, PGMA-based star-like polycations with plentiful hydroxyl groups act as highly efficient miRNA delivery nanovectors for effective applications in heart diseases, Adv. Mater. 28 (2016) 7204–7212.
[33] Y. Zhi, C. Xu, D. Sui, J. Du, F.J. Xu, Y. Li, Effective delivery of hypertrophic miRNA inhibitor by cholesterol-containing nanocarriers for preventing pressure overload induced cardiac hypertrophy, Adv. Sci. 6 (2019) 1900023.
[34] K. Saha, M. Rahimi, M. Yazdani, S.T. Kim, D.F. Moyano, S. Hou, R. Das, R. Mout, F. Rezaee, M. Mahmoudi, V.M. Rotello, Regulation of macrophage recognition through the interplay of nanoparticle surface functionality and protein corona, ACS Nano 10 (2016) 4421–4430.
[35] S. Tenzer, D. Docter, S. Rosfa, A. Wlodarski, J. Kuharev, A. Rekik, S.K. Knauer, C. Bantz, T. Nawroth, C. Bier, J. Sirirattanapan, W. Mann, L. Treuel, R. Zellner, M. Maskos, H. Schild, R.H. Stauber, Nanoparticle size is a critical physicochemical determinant of the human blood plasma corona: a comprehensive quantitative proteomic analysis, ACS Nano 5 (2011) 7155–7167.
[36] K. Preissner, Structure and biological role of vitronectin, Annu. Rev. Cell Biol. 7 (1991) 275–310.
[37] C. Corbo, R. Molinaro, A. Parodi, N.E.T. Furman, F. Salvatore, E. Tasciotti, The impact of nanoparticle protein corona on cytotoxicity, immunotoxicity and target drug delivery, Nanomedicine 11 (2016) 81–100.
[38] A. Zensi, D. Begley, C. Pontikis, C. Legros, L. Mihoreanu, C. Büchel, J. Kreuter, Human serum albumin nanoparticles modified with apolipoprotein A-I cross the blood-brain barrier and enter the rodent brain, J. Drug Target. 18 (2010) 842–848.
[39] A. Zensi, D. Begley, C. Pontikis, C. Legros, L. Mihoreanu, S. Wagner, C. Büchel, H. von Briesen, J. Kreuter, Albumin nanoparticles targeted with Apo E enter the CNS by transcytosis and are delivered to neurones, J. Contr. Release 137 (2009) 78–86.
[40] P. Aggarwal, J.B. Hall, C.B. McLeland, M.A. Dobrovolskaia, S.E. McNeil, Nanoparticle interaction with plasma proteins as it relates to particle biodistribution, biocompatibility and therapeutic efficacy, Adv. Drug Deliv. Rev. 61 (2009) 428–437.
[41] A. Chonn, S.C. Semple, P.R. Cullis, β2-Glycoprotein I is a major protein associated with very rapidly cleared liposomes in vivo, suggesting a significant role in the immune clearance of "non-self" particles, J. Biol. Chem. 270 (1995) 25845–25849.
[42] C. Sacchetti, K. Motamedchaboki, A. Magrini, G. Palmieri, M. Mattei, S. Bernardini, N. Rosato, N. Bottini, M. Bottini, Surface polyethylene glycol conformation influences the protein corona of polyethylene glycol-modified single-walled carbon nanotubes: potential implications on biological performance, ACS Nano 7 (2013) 1974–1989.